Reduced ENSO Variability due to a Collapsed Atlantic Meridional Overturning Circulation

BRYAM ORIHUELA-PINTO,[a,b] AGUS SANTOSO,[a,b,c] MATTHEW H. ENGLAND,[a,d] AND ANDRÉA S. TASCHETTO[a,b]

[a] Climate Change Research Centre, University of New South Wales, Sydney, New South Wales, Australia
[b] Australian Research Council Centre of Excellence for Climate Extremes, University of New South Wales, Sydney, New South Wales, Australia
[c] Centre for Southern Hemisphere Oceans Research, CSIRO Oceans and Atmosphere, Hobart, Tasmania, Australia
[d] Australian Centre for Excellence in Antarctic Science, University of New South Wales, Sydney, New South Wales, Australia

(Manuscript received 14 April 2021, in final form 28 August 2021)

ABSTRACT: Atlantic meridional overturning circulation (AMOC) collapses have punctuated Earth's climate in the past, and future projections suggest a weakening and potential collapse in response to global warming and high-latitude ocean freshening. Among its most important teleconnections, the AMOC has been shown to influence El Niño–Southern Oscillation (ENSO), although there is no clear consensus on the tendency of this influence or the mechanisms at play. In this study, we investigate the effect of an AMOC collapse on ENSO by adding freshwater in the North Atlantic in a global climate model. The tropical Pacific mean-state changes caused by the AMOC collapse are found to alter the governing ENSO feedbacks, damping the growth rate of ENSO. As a result, ENSO variability is found to decrease by ~30% due to weaker air–sea coupling associated with a cooler tropical Pacific and an intensified Walker circulation. The decreased ENSO variability manifests in ~95% less frequent extreme El Niño events and a shift toward more prevalent central Pacific El Niño than eastern Pacific El Niño events, marked by a reduced ENSO nonlinearity and asymmetry. These results provide mechanistic insights into the possible behavior of past and future ENSO in a scenario of a much weakened or collapsed AMOC.

SIGNIFICANCE STATEMENT: The Atlantic meridional overturning circulation (AMOC) has collapsed in the past and a future collapse due to greenhouse warming is a plausible scenario. An AMOC shutdown would have major ramifications for global climate, with extensive impacts on climate phenomena such as El Niño–Southern Oscillation (ENSO), which is the strongest source of year-to-year climate variability on the planet. Using numerical simulations, we show that an AMOC shutdown leads to weaker ENSO variability, manifesting in 95% reduction in extreme El Niño events, and a shift of the ENSO pattern toward the central Pacific. This study sheds light on the mechanisms behind these changes, with implications for interpreting past and future ENSO variability.

KEYWORDS: Atmosphere-ocean interaction; ENSO; Meridional overturning circulation; Teleconnections; Climate variability; Tropical variability

1. Introduction

The Atlantic meridional overturning circulation (AMOC) is an important component of our climate system. It plays a crucial role in the global interhemispheric oceanic heat transport, with implications for both local and global atmospheric circulation and climate. For instance, ocean heat transport associated with the AMOC regulates temperatures and precipitation over Europe (Sutton and Hodson 2005), rainfall over the United States (Enfield et al. 2001), ice mass loss over Greenland (Rainsley et al. 2018), and sea ice coverage over the Arctic (Mahajan et al. 2011). On a global scale, the AMOC has been shown to control Sahel rainfall (Martin et al. 2014) and the mean position of the intertropical convergence zone (ITCZ; Frierson et al. 2013; Marshall et al. 2014). Variations in the AMOC have also caused abrupt climate changes in the past (Rahmstorf 2002; Clement and Peterson 2008), impacting climate on shorter time scales (e.g., interannual and decadal) via changes in Atlantic sea surface temperatures (SST) (Timmermann et al. 2007a; Deser et al. 2010). Another key element of Earth's climate system is El Niño–Southern Oscillation (ENSO), which influences local and global atmospheric circulation in fundamental ways (McPhaden et al. 2006). ENSO is the most important interannual mode of climate variability, causing major changes in temperature and precipitation patterns in the tropics and extratropics (Yeh et al. 2018; Trenberth 2020).

Due to their pronounced influence on global climate, there has been growing interest in understanding how both the AMOC and ENSO will change in the future. At present, there is evidence that the AMOC is slowing down (Bryden et al. 2005; Rahmstorf et al. 2015; Caesar et al. 2018, 2021), and that this slowdown is projected to continue with global warming (Collins et al. 2013). ENSO characteristics have also changed in recent decades (e.g., Freund et al. 2019; Wang et al. 2019), with more frequent extreme ENSO events projected under greenhouse warming (Cai et al. 2020). While complex air–sea

Supplemental information related to this paper is available at the Journals Online website: https://doi.org/10.1175/JCLI-D-21-0293.s1.

Corresponding author: Bryam Orihuela-Pinto, bryamorihuela@gmail.com

DOI: 10.1175/JCLI-D-21-0293.1

© 2022 American Meteorological Society. For information regarding reuse of this content and general copyright information, consult the AMS Copyright Policy (www.ametsoc.org/PUBSReuseLicenses).

Unauthenticated | Downloaded 01/24/24 02:17 AM UTC

feedback processes governing ENSO (Timmermann et al. 2018) contribute to uncertainty in ENSO future projections, changes in the mean state result in some robust elements in the projections (Cai et al. 2020; Yun et al. 2021).

AMOC and ENSO are expected to be important factors controlling global climate in the future. In particular, projections of an AMOC slowdown are robust across global climate models, with a full shutdown considered a possible scenario (Bakker et al. 2016; Liu et al. 2017). In addition, the rates of projected AMOC slowdown in present-day climate models are likely to be underestimated as most models do not include the impact of melting Greenland ice shelves and land ice, which act to further freshen the North Atlantic and weaken the AMOC. There is also evidence in paleoclimate records that suggests that past climate eras have been characterized by a weaker or collapsed AMOC (e.g., Clement and Peterson 2008; Rahmstorf 2002; Clark et al. 2002). Understanding the response of the global climate system to a collapsed AMOC is thus relevant to both future and past climate studies.

There have been several studies that have investigated the influence of an AMOC shutdown on ENSO, but there is still no clear consensus on this topic, and hence further research is required. Dong and Sutton (2007) and Timmermann et al. (2007a) found that the majority of models they used, which contributed to phase 3 of the Coupled Model Intercomparison Project (CMIP3), exhibit an increased ENSO amplitude in response to an AMOC shutdown, which is argued to be related to a weaker annual cycle of the tropical Pacific. A more recent study by Williamson et al. (2018), using a newer model version of that used by Dong and Sutton (2007), found an eastward shift in variability, with no particular amplitude changes despite also presenting a weaker annual cycle.

In this study, we further explore the effect of an AMOC collapse on ENSO. This is achieved by forcing AMOC to shut down in multiple simulations using the Community Earth System Model, version 1.2 (CESM 1.2), coupled global climate model, that is known to simulate ENSO processes and feedbacks well (Deser et al. 2012; Capotondi 2013; Taschetto et al. 2014). The overall global changes obtained in these simulations in response to an AMOC shutdown agree with previous literature (Vellinga and Wood 2002; Zhang and Delworth 2005; Stouffer et al. 2006; Cheng et al. 2007; Wu et al. 2008; Orihuela-Pinto et al. 2022) starting from a widespread Northern Hemisphere cooling (centered in the North Atlantic), which creates a stronger interhemispheric temperature gradient. This interhemispheric temperature gradient has further effects associated with the perturbed meridional energy balance, which includes a southward shift of the ITCZ and an intensified northern Hadley cell. The focus of this study, however, will be on how these well-known global changes can ultimately affect ENSO behavior and variability. We also explore the resultant changes in ENSO diversity, which has not been examined in previous studies.

This study is organized as follows: In section 2 we describe the model and experimental design. Section 3 explores how an AMOC collapse changes the tropical Pacific mean state and variability. Changes in ENSO feedbacks are explored in section 4. In section 5 we show how changes in feedbacks affect ENSO diversity. Finally, a discussion and the major conclusions are presented in section 6.

2. Methods

a. The global climate model

The global climate model used in this study is the National Centre for Atmospheric Research (NCAR) CESM 1.2, a fully coupled model comprising atmospheric, oceanic, land, and sea ice models (Gent et al. 2011). The atmospheric component is the Community Atmospheric Model, version 4 (CAM4), configured at 1.9° × 2.5° spatial resolution and a hybrid sigma-pressure vertical coordinate with 26 layers in the vertical grid. The land component is the Community Land Model, version 4 (CLM4), that runs on the same grid as the atmospheric model. The ocean model is the Parallel Ocean Program, version 2 (POP2), set with a displaced-pole in the Northern Hemisphere over Greenland at 80°N, 40°W. The horizontal grid is nearly uniform in longitude (~1.13°) and variable in latitude (0.27° at the equator, increasing to 0.65° at 60°N in the western North Pacific), with 60 vertical levels varying in thickness from 10 m near the surface to 250 m at depth. The sea ice component is the Community Ice Code, version 4 (CICE4), which runs on the same grid as the ocean model. All model components iterate via a coupling architecture that allows the exchange of freshwater, momentum, and heat fluxes between components. The model has been shown to have a good representation of the AMOC in a modern era setting (Danabasoglu et al. 2012). Additionally, it has been shown to have a good representation of ENSO (Deser et al. 2012) and its diversity (Capotondi 2013; Taschetto et al. 2014), as well as interbasin coupling between the Atlantic and the Pacific (Orihuela-Pinto et al. 2022). Figure S1 and Table S1 provide information on the model's biases and key metrics of tropical Pacific SSTs. The cold tongue bias for this model is relatively small (on the order of 0.1°C) compared with other models (on the order of 1°C; e.g., Santoso et al. 2019). Having a reduced cold tongue bias makes this model suitable for the analysis of ENSO feedbacks (Kim et al. 2014). Furthermore, the SST variability amplitude, and skewness (with monthly mean removed) are reasonably well represented, relative to many CMIP5 and CMIP6 models that even simulate a wrong sign in skewness (McKenna et al. 2020).

b. Experimental design

First, we spin up a preindustrial control climate for 1000 years and from there, branch a control experiment (AMOC-on) for an extra 250 years. We also run an ensemble of perturbed meltwater experiments (AMOC-off) branched from the 1000 years control run. The ensemble members-are initialized every 10 years branching off the control (Fig. 1), consisting of a set of 5 × 100-yr simulations with a constant surface freshwater forcing of 1 Sv (1 Sv ≡ 10^6 m^3 s^{-1}) applied over the North Atlantic (50°–70°N). No flux adjustments are used in either simulation. The analysis of AMOC-off corresponds to the last 50 years of each perturbed run, at which point the AMOC has collapsed and the climate response is in

Unauthenticated | Downloaded 01/24/24 02:17 AM UTC

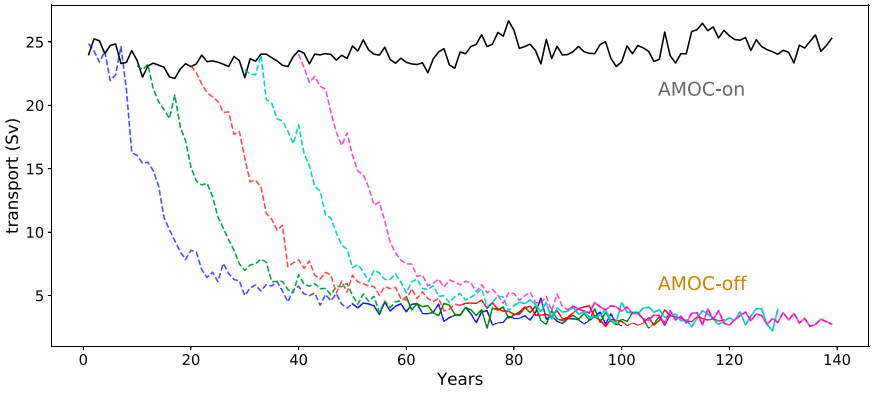

FIG. 1. AMOC transport (Sv) for the AMOC-on (black) and AMOC-off runs (colors). The last 50 years in each of the AMOC-off runs (solid lines) are the periods where the AMOC is considered to be shutdown.

equilibrium (solid lines in Fig. 1). Our results are presented in terms of ensemble means, with intermember spread shown as applicable. Additionally, unless specified otherwise, all ENSO-related analyses are based on variability with the seasonal cycle removed.

3. Tropical Pacific mean state and variability

The most evident response to the AMOC shutdown in the Northern Hemisphere is an overall cooling, caused by the suppression of northward oceanic heat transport (Fig. 2a). This cooling is most pronounced in the North Atlantic Ocean where the freshwater forcing directly affects deep-water formation and thus the meridional ocean heat transport. The Southern Hemisphere exhibits an overall warming of weaker magnitude (Fig. 2a). The precipitation changes (Fig. 2b) follow the temperature change pattern, with overall increased precipitation in the Southern Hemisphere and a reduction in the Northern Hemisphere, suggesting a southward displacement of the ITCZ that features decreased intensity in the equatorial region.

However, unlike the Atlantic basin, the Pacific interhemispheric temperature change is less asymmetric about the equator. Instead, the cooler temperatures, which are more pronounced in the eastern Pacific, extend into the South Pacific, accompanied by an intensification of the northeasterly trade winds (Fig. 2a). The origin of this temperature asymmetry with respect to the equator in the Pacific is a reorganization of the zonal atmospheric circulation, that is, the Walker circulation (Orihuela-Pinto et al. 2022). More specifically, enhanced convection triggered by surface warming in the equatorial South Atlantic drives an acceleration of the Pacific Walker cell. The stronger Pacific Walker cell is expressed at the surface as enhanced trade winds, which contributes to the equatorial Pacific cooling (Orihuela-Pinto et al. 2022, their Fig. 5b). The trade wind acceleration in the Pacific drives further changes in the mean state of the ocean through increased evaporation, enhanced upwelling that induces mixing, and upper-ocean heat content recharge via equatorward Sverdrup transport (ocean interior warming). This leads to a deepening of the mixed layer and thermocline depth in both the central and western equatorial Pacific (Fig. 3), and thus an overall reduction of equatorial Pacific Ocean stratification.

It is worth noting that while the anomalous interhemispheric SST pattern is a robust feature across studies (Timmermann et al. 2007a; Dong and Sutton 2007; Williamson et al. 2018), the changes occurring within the tropical Pacific appear to be model dependent. For instance, the surface cooling in our model extends throughout the tropical Pacific, while in other models some warming occurs in the equator and off-equatorial regions, translating to differences in the zonal structure of winds and thermocline (Timmermann et al. 2007a; Dong and Sutton 2007; Williamson et al. 2018). A diverse response is likely due to a delicate balance between feedback processes in the equatorial region where air–sea coupling is strong. The coupled feedbacks are also sensitive to processes outside the Pacific basin, the level of which varies across models (e.g., Kajtar et al. 2017; Cai et al. 2019). Nonetheless, a weakened meridional SST gradient over the eastern equatorial Pacific associated with the Northern Hemisphere cooling seems to be consistent across models, and this tends to weaken the SST annual cycle (Xie 1994; Timmermann et al. 2007a).

The seasonality of the mean-state changes (Fig. 4) shows that while the trade winds are intensified in the equatorial Pacific during all months, this intensification is not uniform across seasons. In the central/western Pacific, the strongest trade winds intensification occurs around boreal spring along with the maximum increase in zonal temperature gradient, followed by a maximum in thermocline deepening in the subsequent season. The minimum in trade wind intensification occurs by the end of the boreal summer and start of fall, accompanied by a decrease in zonal SST gradient; a minimum in thermocline deepening follows. Note that the model's seasonal cycle (Figs. 4a and 6a) is reasonable relative to other modern climate models (e.g., Song et al. 2020; Liao et al. 2021), including those examined by Timmermann et al. (2007a; see their Fig. 2), some of which exhibit strong semiannual cycle in the eastern equatorial Pacific.

Unauthenticated | Downloaded 01/24/24 02:17 AM UTC

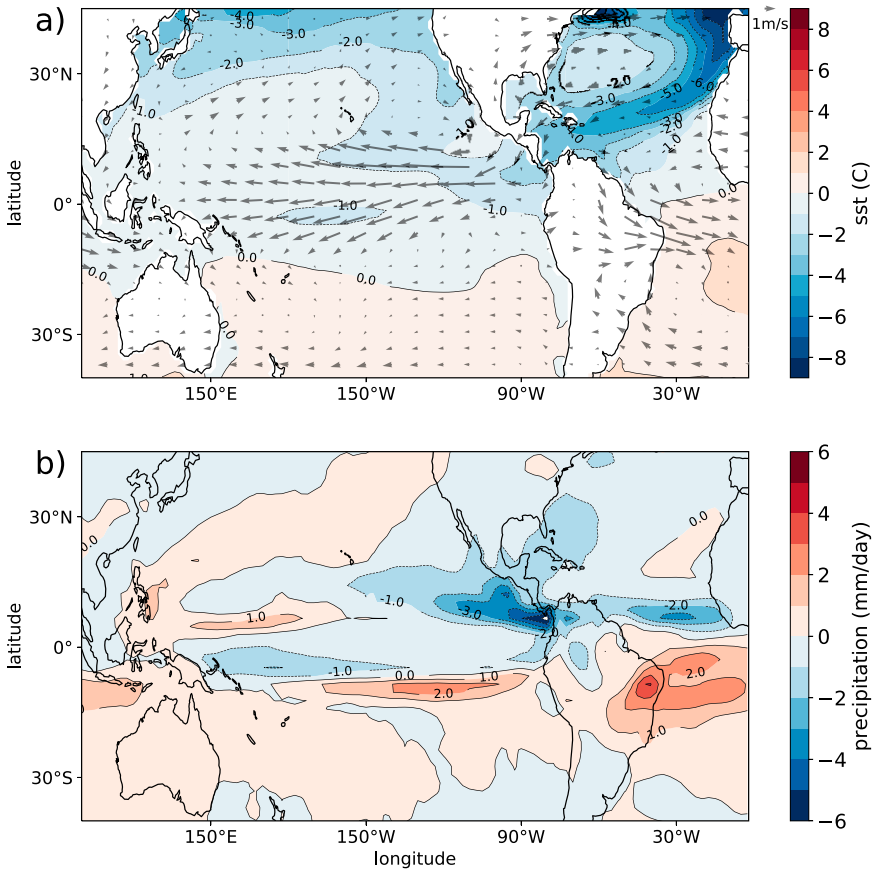

FIG. 2. Mean-state changes (ensemble mean of AMOC-off minus AMOC-on) in (a) sea surface temperature (°C; shading) and 850-hPa winds (m s^{-1}; vectors), and (b) precipitation (mm day^{-1} shading).

Aside from the mean-state changes, there are also important variability changes in the Pacific basin. To the east of the date line, there is a notable reduction in SST variability, exhibiting an ENSO-like spatial pattern (Fig. 5a), peaking around the Niño-3.4 region (yellow box in Fig. 5a). The SST variability in the eastern Pacific (180°–280°E, 5°S–5°N) reduces by approximately 30%. Associated with these changes, there is a reduced precipitation variability that peaks just to the west of the maximum SST variability reduction (Fig. 5b), as would be expected from the nonlinear response of the atmosphere to equatorial Pacific SST anomalies (e.g., Hoerling et al. 1997; Takahashi and Dewitte 2016). In particular, a cooler than normal sea surface exerts a stronger impact in the vicinity of the western Pacific warm pool than in the cold tongue region. In addition, the seasonality of the SST variability changes in the area with maximum reduction (Niño-3.4) exhibits a cooling across all months, with the largest temperature decrease occurring in boreal winter (Fig. 5c), when ENSO usually peaks. The Niño-3.4 power spectra are shown in Fig. 5d, indicating that the ENSO periodicity has reduced from ~5 to 3 years, with a notably reduced power.

Previous studies have linked changes in ENSO variability to changes in seasonal cycle via the nonlinear frequency entrainment mechanism (Chang et al. 1994; Liu 2002; Timmermann et al. 2007b), which suggests that a decrease in ENSO variability would be linked to an enhanced seasonal cycle, and vice versa. In our model experiments, this relationship is the opposite, as a

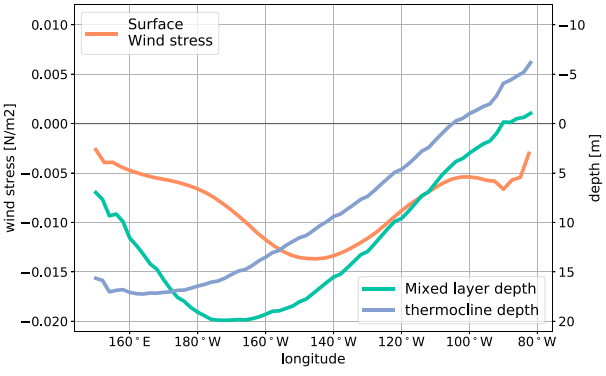

FIG. 3. Mean-state changes (AMOC-off ensemble mean minus AMOC-on) in equatorial (5°S–5°N) wind stress (orange line), 20°C isotherm or thermocline depth (blue line), and mixed layer depth (green line). Note the *y* axis on the right is inverted for easier visualization with the other variables.

Unauthenticated | Downloaded 01/24/24 02:17 AM UTC

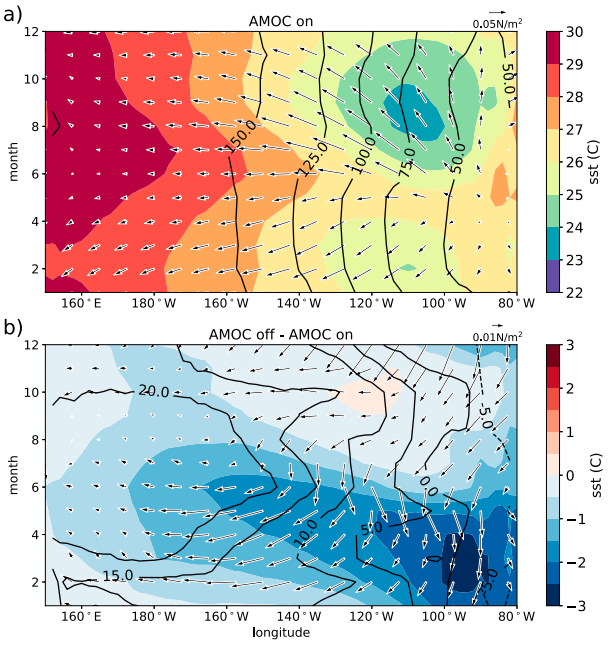

FIG. 4. Monthly equatorial (5°S–5°N) mean-state SST (°C; shading), thermocline depth (m; contour), and wind stress (N m^{-2}; vectors) in the Pacific of (a) AMOC-on run and (b) its change (ensemble mean of AMOC-off ensemble mean minus AMOC-on) when AMOC shuts down.

reduced ENSO variability is accompanied by a weakened annual cycle (Fig. 6). The difference between the annual cycles of the experiment and control runs (Fig. 6b) shows a trade wind intensification in the central/west Pacific during boreal spring preceding a deepening of the west Pacific thermocline in the following months. Additionally, trade wind weakening occurs around the end of boreal winter, followed by a shallowing of the thermocline. These changes are opposite to the control climatological annual cycle (Fig. 6a). Likewise, the SST change shows an opposite behavior to the AMOC-on annual cycle, with cooling in the east Pacific from January to May and warming from May to December.

Thus, in response to an AMOC shutdown, a weakening of the annual cycle was found along with reduced ENSO variability. To understand the cause of the reduced ENSO variability in the AMOC-off runs, we next explore how the feedback processes governing ENSO behavior change in the perturbed experiments.

4. ENSO feedbacks

a. *Linear stability analysis*

To assess how the AMOC collapse affects ENSO feedbacks, we utilize the Bjerknes stability (BJ) index (Jin et al. 2006). The BJ index is a framework for assessing ENSO dynamics based on the recharge-oscillator paradigm (Jin 1997). The BJ index quantifies the linear stability of the coupled ENSO mode by formulating the ENSO growth rate in terms of the strength of the equatorial Pacific air–sea feedback

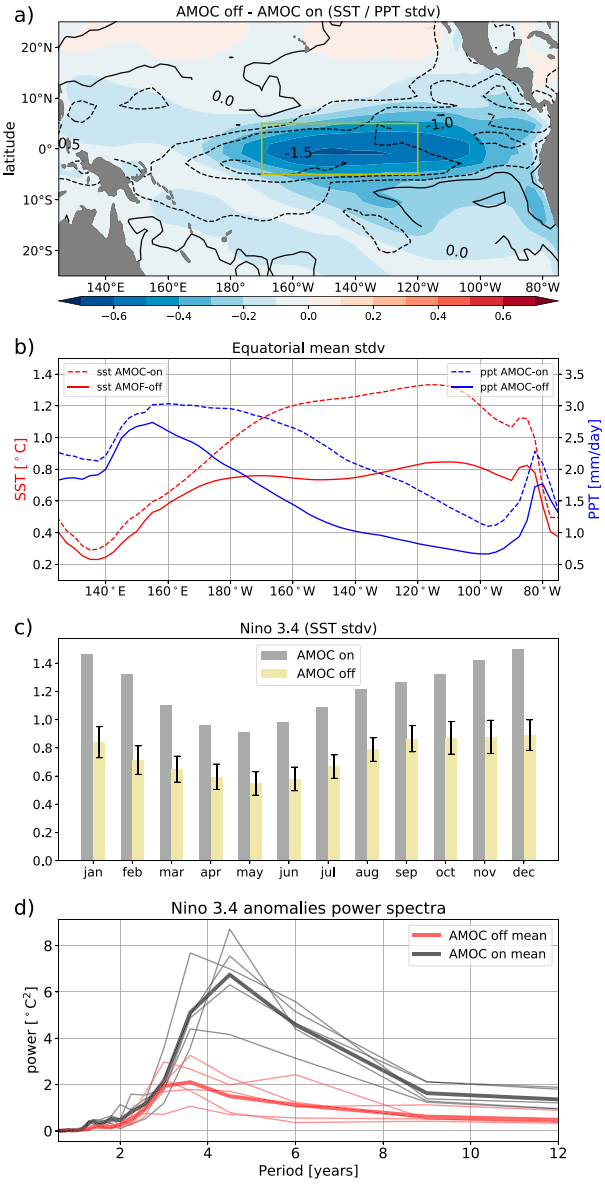

FIG. 5. (a) Spatial distribution of the difference in standard deviation of the SST anomalies (°C; shading) and precipitation anomalies (mm day^{-1}; contour) between the AMOC-off (ensemble mean) and AMOC-on runs. (b) Standard deviation of SST anomalies (red) and precipitation anomalies (blue) in the equatorial Pacific (5°S–5°N) for both the AMOC-on (dashed) and ensemble mean of AMOC-off (solid). (c) Standard deviation of SST in the Niño-3.4 region [yellow box in (a)] for the AMOC-on (250 years) and ensemble mean of AMOC-off runs (5 members × 50 years; whiskers show members spread). (d) Power spectra of Niño-3.4 SST anomalies in AMOC-on for different 50 years chunks (thin black lines) and last 50 years of each of the AMOC-off run members (thin red lines) and their respective means (thick lines).

processes and mean state that lead to a dampening or growth of ENSO and hence its SST variability. Here we use the BJ index formulation as applied in Lübbecke and McPhaden (2013), which is based on Jin et al. (2006) with modifications

Unauthenticated | Downloaded 01/24/24 02:17 AM UTC

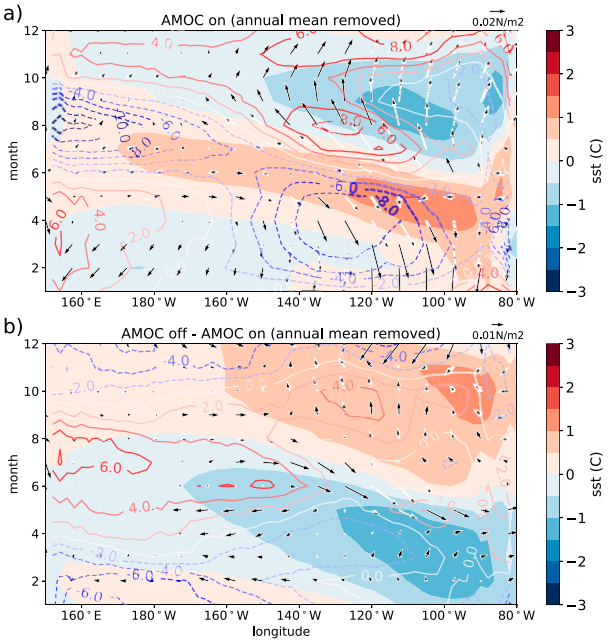

FIG. 6. As in Fig. 4, but with the mean state (annual mean) removed from each of the runs.

from Kim and Jin (2011) and Stein et al. (2010). The total BJ index is represented as a linear combination of terms that contribute to the growth or damping of ENSO:

$$2I_{\mathrm{BJ}} = \underbrace{-\left(\frac{\langle\overline{u}\rangle_E}{L_x} + \frac{\langle -2y\overline{v}\rangle_E}{L_y^2} + \frac{\langle\overline{w}\rangle_E}{H_m}\right)}_{\mathrm{DD}}\underbrace{-\alpha}_{\mathrm{TD}} + \underbrace{\mu_a\beta_u\left\langle -\frac{\partial\overline{T}}{\partial x}\right\rangle_E}_{\mathrm{ZA}} + \underbrace{\mu_a\beta_h\left\langle\frac{H(w)\overline{w}}{H_m}a_h\right\rangle_E}_{\mathrm{TC}} + \underbrace{\mu_a\beta_w\left\langle -\frac{\partial\overline{T}}{\partial z}\right\rangle_E}_{\mathrm{EK}}, \quad (1)$$

where all mathematical symbols used in Eq. (1) are outlined in Table 1. The reader is also referred to Lübbecke and McPhaden (2013) for further details on the formulation of terms in Eq. (1). The damping processes are the dynamical damping (DD) and the thermodynamical damping (TD); the former represents damping by the mean advection, and the latter is damping by the net air–sea heat flux across the ocean surface. The main amplifying (positive) feedbacks are the zonal advective (ZA), thermocline (TC), and Ekman (EK) feedbacks. The zonal advective feedback describes the effect of the winds in driving anomalous zonal currents that act on the climatological zonal SST gradient via temperature advection. The Ekman feedback describes the effect of anomalous wind-driven upwelling acting on the mean vertical temperature gradient. The thermocline feedback quantifies the effect of anomalous zonal wind stress acting on the thermocline slope, which in turn affects surface and subsurface temperatures via mean upwelling.

The three amplifying feedbacks (ZA, TC, and EK) are represented as products of the mean state and coupling coefficients that capture the feedback between the surface wind with SST, upper-ocean currents, and thermocline. The BJ index is particularly useful for our purposes since it provides a means to understanding how the mean-state changes will affect ENSO behavior, as used in previous studies (e.g., Kim and Jin 2011; Santoso et al. 2012).

TABLE 1. Bjerknes index terms and their formulation. Here $\langle\rangle_E$ represents area averaging over the east equatorial Pacific (180°–280°E, 5°S–5°N). The overbar represents time mean. The terms u and v represent the zonal and meridional currents in the mixed layer, w is the vertical current at the base of the mixed layer, and T is the surface mixed-layer temperature. The terms L_x and L_y are the zonal and meridional extents of the averaged areas whereas H_m is the mixed layer depth. The factor $2y/L_y$ comes from the assumption that the structure of the SST anomalies is Gaussian-like with an e-folding decay scale of L_y. The thermodynamical damping term α is calculated as the regression of the heat flux anomalies onto the SST anomalies and is a linear combination of its different components: shortwave (α_{SW}), longwave (α_{LW}), latent heat (α_{LH}), and sensible heat (α_{SH}). The term μ_a is the linear regression coefficient between equatorial Pacific wind stress anomalies against east Pacific SST anomalies; β_u, β_h, and β_w are obtained by regressing u, thermocline slope, and w anomalies (respectively) against equatorial Pacific surface wind stress anomalies. The term a_h is the linear regression coefficient of subsurface temperatures onto east Pacific thermocline depth. Finally, $H(x)$ is a step function, which ensures that only upward vertical advection is taken into account.

Term	Formula
Dynamical damping (DD)	$-\left(\frac{\langle\overline{u}\rangle_E}{L_x} + \frac{\langle -2y\overline{v}\rangle_E}{L_y^2} + \frac{\langle\overline{w}\rangle_E}{H_m}\right)$
Thermodynamical damping (TD)	$-\alpha$
Zonal advective feedback (ZA)	$\mu_a\beta_u\left\langle -\frac{\partial\overline{T}}{\partial x}\right\rangle_E$
Thermocline feedback (TC)	$\mu_a\beta_h\left\langle\frac{H(w)\overline{w}}{H_m}a_h\right\rangle_E$
Ekman feedback (EK)	$\mu_a\beta_w\left\langle -\frac{\partial\overline{T}}{\partial z}\right\rangle_E$

The total BJ index along with its components and their change between simulations are shown in Figs. 7a and 7b, respectively. The total BJ index reduction in the AMOC-off simulations compared to the AMOC-on is ~25%, consistent with the ~30% reduction in ENSO variability as noted in section 3. Further decomposition of its individual components shows that the damping is primarily due to a weakening of the positive feedbacks, especially the TC (27%) and ZA (18%) feedbacks (the decrease in the Ekman feedback is not significant). The DD shows no significant change, and the TD is reduced by 45% (i.e., less negative) thus partially offsetting the decrease in the positive feedbacks and contributing to a more positive BJ index.

The decrease in thermodynamical damping is mainly due to a reduction in the sensitivity of latent heat flux and shortwave radiation to SST variations in the equatorial Pacific (Fig. 7b). This is expected as under a cooler mean

Unauthenticated | Downloaded 01/24/24 02:17 AM UTC

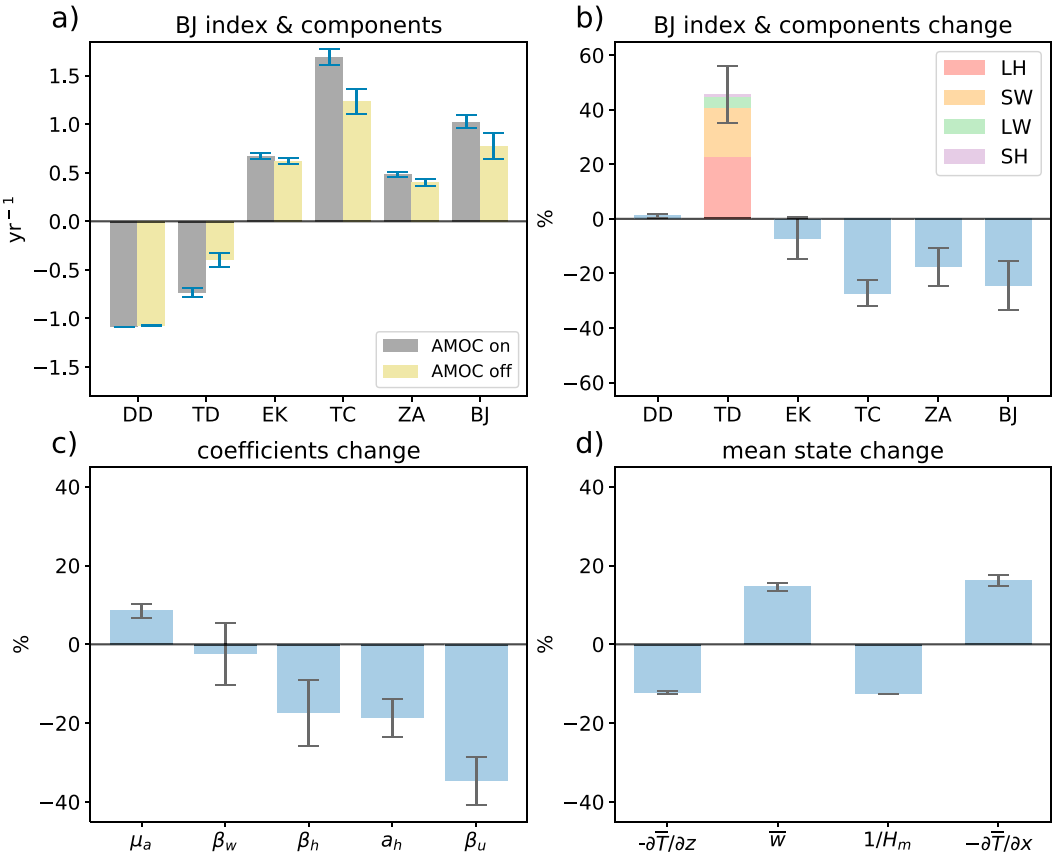

FIG. 7. (a) Total BJ index and its terms (yr^{-1}; see Table 1 for description) with whiskers marking one standard deviation above and below the mean and (b) their percentage change including components contribution for TD. The percentage change in (c) coupling and (d) mean-state coefficients. For this analysis, equivalent periods from the AMOC-off run and AMOC-on runs were taken to make it comparable and have similar sample size for regressions.

state, SST variations are not as efficient in triggering changes in atmospheric convection, thus cloud generation and evaporative cooling, which tend to damp El Niño warm surface anomalies.

To examine the mechanisms behind the weakening of the positive feedbacks (Figs. 7a,b), we analyze the changes in their various governing factors (Figs. 7c,d). The three positive feedbacks have in common the coupling of the surface winds and SST (μ_a), which increases by 9%; however, in all cases there are other factors that offset this effect, making the final feedback change negative.

For the thermocline feedback, the weakening is caused mainly by both reduced coupling between the surface winds and thermocline depth (β_h) and also reduced sensitivity of the thermocline changes on subsurface temperatures (a_h). The reduced coupling may appear to be moderated by an increase in mean upwelling ($\overline{w}$) linked to the enhanced climatological trade winds (Figs. 2a, 3), but at the same time the mixed layer depth increases, thus countering the increase in upwelling. In the case of the zonal advective feedback, the main contributor to its weakening is a reduction in the coupling between the surface winds and the zonal ocean current (β_u), offset partially by an increase in the climatological zonal SST gradient [$-(\partial\overline{T}/\partial x)$]. Finally, the Ekman feedback shows a negative contribution due to a stronger vertical temperature gradient [$-(\partial\overline{T}/\partial z)$] and a weaker coupling between surface winds and upwelling (β_w); however, the latter has strong interensemble member variability, which ultimately renders the Ekman feedback reduction to be less significant. The reduced air–sea coupling could be due in part to the increased mixed layer depth (i.e., $1/H_m$ decreases) in the AMOC-off scenario, wherein more energy would be required for the atmosphere to influence a thicker mixed layer.

b. SST–precipitation coupling

The existence of a convective SST threshold in the tropics is a well-known phenomenon (Johnson and Xie 2010), which is particularly relevant both for strong ENSO events (Takahashi and Dewitte 2016) and for controlling ENSO diversity (Geng et al. 2020). When the tropical SSTs exceeds the convective threshold, the atmospheric response (e.g., precipitation, winds) to a relatively small increase in SST becomes much stronger, causing an anomalously warm event to develop at a faster rate. Hence, in order to further understand ENSO

Unauthenticated | Downloaded 01/24/24 02:17 AM UTC

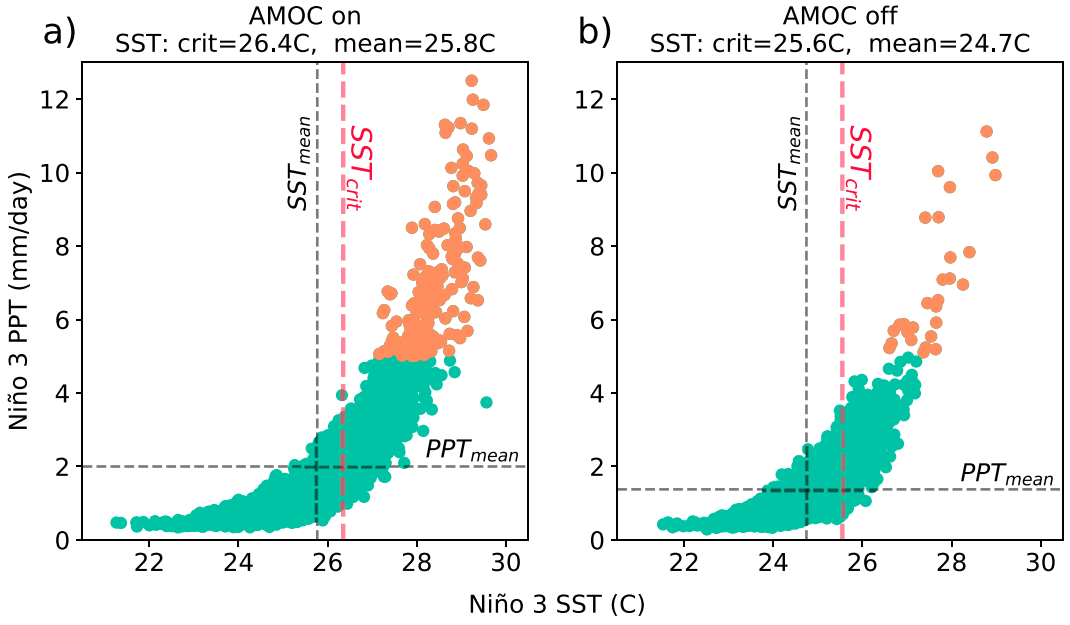

FIG. 8. Scatterplots of monthly SST (°C) vs precipitation (mm day^{-1}) in the Niño-3 region (yellow box in Fig. 5a) for the (a) AMOC-on and (b) AMOC-off simulations. Orange dots represent cases when precipitation > 5 mm day^{-1}. The December–February average of this values was calculated to quantify extreme El Niño cases (Cai et al. 2014) and found that its frequency decreased by ~95%. For calculating the critical temperature (red vertical dashed line) for convection we used the Johnson and Xie (2010) method, which finds the temperature at which the mean precipitation exceeds 2 mm day^{-1}. The mean SST and precipitation are also shown as black vertical and horizontal dashed lines, respectively.

changes, aside from the linear feedback analysis made in the previous section, it is important to assess how this nonlinear feedback changes in the AMOC-off world.

The relationship between SST and precipitation in the east Pacific shown in Fig. 8 reveals that in both the AMOC-on and AMOC-off cases, the rate of precipitation increase per SST increase is much faster above ~26°C. This implies that the nonlinear feedback between the ocean and the atmosphere is present. However, due to the decrease in mean SST and its variability in the AMOC-off experiment, there is much less likelihood of SST surpassing the convective threshold. Hence, the frequency of extreme El Niño events characterized by occurrences of precipitation exceeding 5 mm day^{-1} (Cai et al. 2014) in boreal winter (December–February average, when ENSO peaks) reduces by 95% in AMOC-off. When comparing the convective threshold, it decreases from 26.4°C in the AMOC-on simulation (Fig. 8a) to 25.6°C in the AMOC-off runs (Fig. 8b). Yet, there are less occurrences of strong El Niño events, as it is harder to shift atmospheric convection to the usually cold equatorial Pacific (i.e., the cold tongue region) due to enhanced meridional and zonal SST gradients (Cai et al. 2017). Thus, the reduced ENSO variability in AMOC-off is also associated with the less frequent extreme El Niño events.

5. ENSO diversity

ENSO events come in diverse "flavors" that fall between two typical spatial structures: either eastern Pacific (EP) ENSO, with peak SST anomalies in the eastern Pacific, or central Pacific (CP) ENSO with maximum SST anomalies in the central Pacific (e.g., Capotondi et al. 2015; Santoso et al. 2019). Understanding these ENSO types is important because the particularities of their spatial patterns influence their impacts and teleconnections. It is thus of interest whether the reduced ENSO variability in AMOC-off involves changes to the prevalence of these two types of ENSO events. To assess the different ENSO types, we used the first two principal modes (PC1 and PC2) of an empirical orthogonal function (EOF) analysis of monthly SST anomalies and the rotated PC1 (E index) and PC2 (C index), defined as

$$\text{E index} = \frac{\text{PC1} - \text{PC2}}{\sqrt{2}}; \quad \text{C index} = \frac{\text{PC1} + \text{PC2}}{\sqrt{2}}. \tag{2}$$

The E and C indices in Eq. (2) describe the eastern and central Pacific ENSO regimes, respectively (Takahashi et al. 2011). The spatial pattern for each of these indices is shown in Fig. 9. The explained variance by PC1 (Figs. 9a,c), which depicts the classical ENSO pattern, in AMOC-off, is reduced (73% AMOC-on to 67% AMOC-off). In the case of PC2 (Figs. 9b,d), which depicts an east–west anomaly structure, the explained variance does not change much (7% AMOC-on to 8% AMOC-off), compared to the AMOC-on scenario. The spatial patterns associated with PC1 and PC2 for AMOC-on and AMOC-off are rather similar, with the main difference being a reduction in their loadings everywhere in AMOC-off. Additionally, there is a westward extension in the EOF patterns consistent with the westward trade wind intensification along the equatorial Pacific (Fig. 2a); this change is also reflected in the E and C spatial patterns.

Unauthenticated | Downloaded 01/24/24 02:17 AM UTC

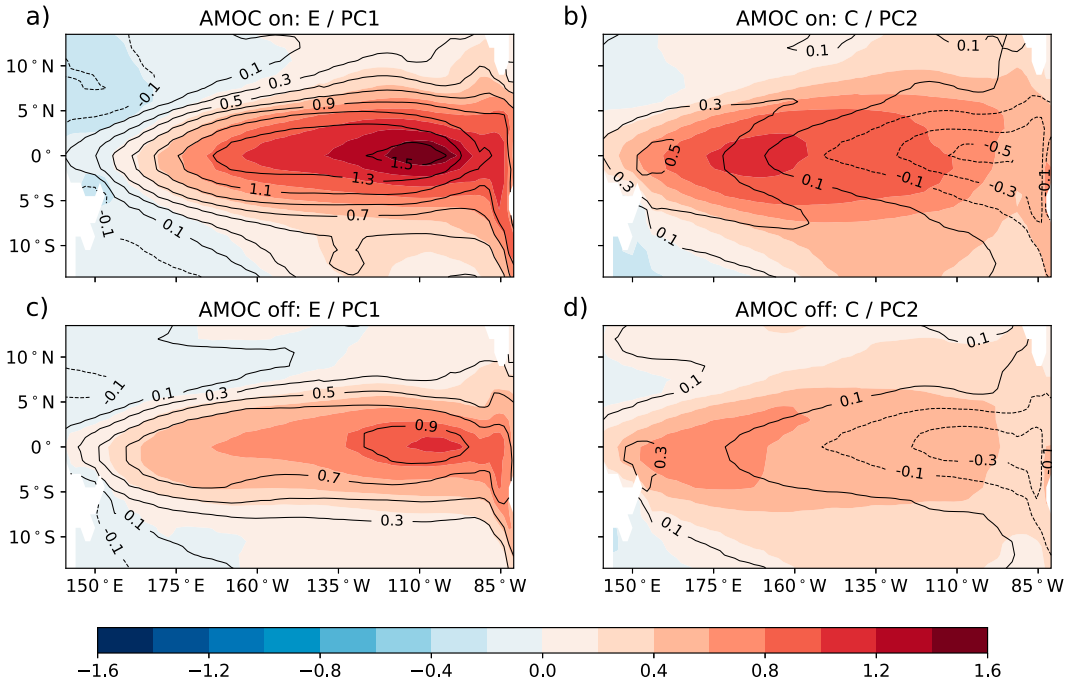

FIG. 9. Spatial pattern of linear regression coefficients between the SST anomalies and (a) E index and (b) C index (shading), for the AMOC-on experiment. (c),(d) As in (a) and (b), but for the AMOC-off simulations. Contours show the regression patterns for PC1 and PC2.

We next use the E and C indices to determine the frequency of EP and CP events (Fig. 10). In the AMOC-on run the proportion of EP and CP events is similar to that seen in observations, with the CP events being more frequent than the EP ones (Fig. 10c). The proportion of EP to CP events reduces in the AMOC-off simulations due to a 32% decrease in the frequency of EP events and a 15% increase in CP frequency. This is in agreement with the change in ENSO feedbacks discussed in section 4. The thermocline feedback is a key mechanism for EP ENSO, since the eastern Pacific SSTs are more sensitive to changes in thermocline depth due to the climatologically shallow thermocline there (Kug et al. 2009; Yu et al. 2010; Xie and Jin 2018). In the central Pacific, the most influential positive feedback is the zonal advective

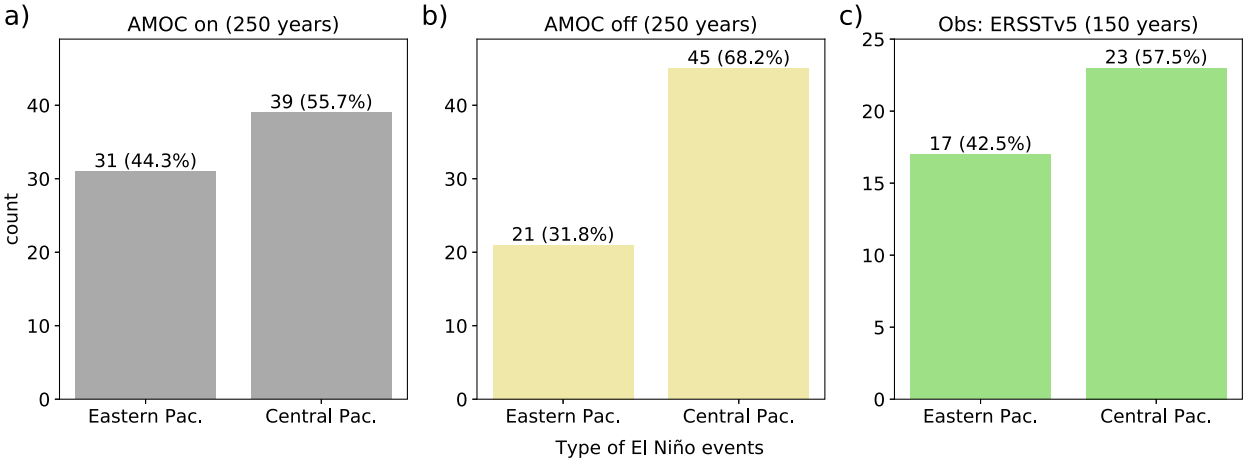

FIG. 10. Count of EP and CP El Niño events and their proportions for the (a) AMOC-on, (b) AMOC-off, and (c) observations (ERSSTv5, years 1870–2020; Huang et al. 2017). The observations period includes preanthropogenic era and coincides with the HadISST period (Rayner et al. 2003), which shows similar results. An EP and CP event is considered when the averaged October–March E and C indices exceed one standard deviation, respectively. The first 250 years of AMOC-on and the 5 members × 50 years for the AMOC-off cases were analyzed.

Unauthenticated | Downloaded 01/24/24 02:17 AM UTC

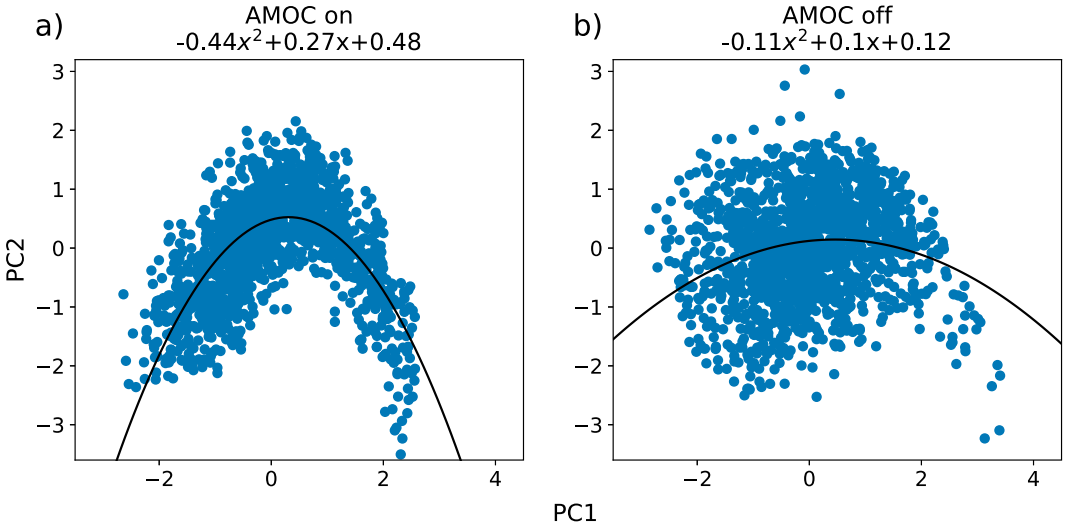

FIG. 11. October–March monthly PC1 vs PC2 with their quadratic fit for (a) AMOC-on and (b) AMOC-off simulations. Same years used as for Fig. 10.

feedback given the strong zonal SST gradient (Kug et al. 2009; Yu et al. 2010; Xie and Jin 2018). This zonal advective feedback is reduced in the AMOC-off scenario; however, its effect is offset by the reduction in thermal damping, which has a stronger role in CP events (Kang and Kug 2002).

Finally, in Fig. 11 we illustrate the monthly PC1 and PC2 relationship in the months from October to March (which possess the highest ENSO related variability). These two indices have a quadratic relationship $\{\mathrm{PC2}(t) = \alpha[\mathrm{PC1}(t)]^2 + \beta[\mathrm{PC1}(t)] + \gamma\}$ that accounts for the ENSO nonlinearity, which in turn gives rise to event diversity. Using α as a measure of the nonlinearity (e.g., Karamperidou et al. 2017; Cai et al. 2018), we found that it has been reduced in AMOC-off, which is consistent with the decrease in extreme events as discussed above.

6. Discussions and conclusions

We investigated how an AMOC collapse affects ENSO behavior using a coupled general circulation model. We ran simulations with preindustrial conditions where freshwater is added in the North Atlantic to force an AMOC shutdown (AMOC-off). It is found that the equatorial Pacific SST and ENSO variability are reduced once the AMOC has collapsed. The AMOC shutdown has global impacts, so it is possible that changes in other tropical basins' variability, and their interactions with the Pacific (Cai et al. 2019), and/or Pacific meridional modes (which act as precursors to ENSO; Chang et al. 2007; Zhang et al. 2014) contribute to the change in ENSO. Although in this study we do not focus on changes to other modes of variability, we note that SST variability changes in other basins are comparatively small (Fig. S2 in the online supplemental material). In addition, most regions exhibit reduced variability, which is likely a consequence of a weakened ENSO, and thus the impact on ENSO is also expected to be reduced. Weaker Pacific meridional modes (PMM) in a cooler climate of AMOC shutdown are in line with the argument of more energetic Pacific meridional modes and linkage with ENSO in a warmer climate due to enhanced wind–evaporation–SST feedback that governs PMM (Liguori and Di Lorenzo 2018). Hence, we conclude that most of the Pacific variability changes are due to the AMOC shutdown.

The ENSO variability reduction contradicts previous studies that found an increase in ENSO variability after an AMOC collapse due to a meltwater pulse in the North Atlantic (Dong and Sutton 2007; Timmermann et al. 2007a; Liu et al. 2014). The supporting argument in these past studies was based on the nonlinear frequency entrainment mechanism, in which a decrease in the seasonal cycle should lead to an increase in ENSO variability. A study by Williamson et al. (2018) further adds diversity to these results by finding an eastward shift of ENSO variability without significant change in amplitude, despite also presenting a weaker annual cycle. In our case the seasonal cycle also decreases, yet we found a notable decrease in ENSO variability; implying that a different mechanism must be at play. Previous studies have also suggested a positive correlation between ENSO variability change and seasonal cycle change in response to external forcing, in contrast to the nonlinear frequency entrainment mechanism (e.g., Emile-Geay et al. 2016; Karamperidou et al. 2020).

We find instead that the mechanism for the ENSO variability reduction in AMOC-off stems from changes in the mean state of the tropical Pacific that alter the ENSO governing feedbacks. Most models that were used in previous studies show an enhanced ENSO variability but exhibit diverse mean-state changes across the models. For instance, Dong and Sutton (2007) obtained a central Pacific warming and enhanced trade winds. Among the models used by Timmermann et al. (2007a), there are a couple of models (CCSM2 and CCSM3) with thermocline deepening and increased trade winds, but less extensive surface cooling than in our model. For these models, the frequency entrainment mechanism was proposed to account for the stronger ENSO variability. In another model (ECHAM5-OM1),

Unauthenticated | Downloaded 01/24/24 02:17 AM UTC

Timmermann et al. (2007a) found thermocline shoaling and weaker trade winds that are consistent in explaining the enhanced ENSO amplitude as in our case but in the opposite sense. Moreover, Williamson et al. (2018) found central Pacific warming, weakened trade winds, and thermocline deepening but no appreciable change in the ENSO amplitude, attributed to the overcompensating effect of reduced stochasticity and negative feedback. Thus, the reasons for changes in ENSO variability can vary from model to model, and in our model mean-state changes are the key factor.

To assess the impact of the mean-state changes on the ENSO feedbacks in our experiment, we implemented the Bjerknes stability index for ENSO (Jin et al. 2006) and found that the main underlying cause is the weakening of the coupling between the surface winds and upper-ocean changes, particularly the zonal currents and thermocline depth variations. This is likely in part due to the deepening of the mean mixed layer in AMOC-off, associated with the enhanced climatological trade winds, thus increasing the energy required from the surface winds to drive upper-ocean changes. Taken together, this causes a weakening in the positive feedbacks that comprise the growth of ENSO. A study by Timmermann et al. (2005) utilizing intermediate complexity models suggested a reduced ENSO variability in response to a North Atlantic meltwater pulse that made its way to the tropical Pacific via the Indian Ocean due to a global ocean wave adjustment mechanism (Cessi et al. 2004). This was shown to deepen the equatorial Pacific thermocline that leads to a weaker ENSO reduction, in agreement with our results. However, unlike the Timmermann et al. (2005) experiment, the thermocline deepening in our fully coupled model does not appear to reach the eastern Pacific (Fig. S3; cf. Fig. 4 of Timmermann et al. 2005) and is not purely due to the global wave adjustment, but also to the influence of enhanced Pacific trade winds.

Despite the ENSO response being different to some previous model studies, our results are consistent with paleo studies that suggest that similar mechanisms and features in tropical Pacific behavior might have played out in the past. In particular, these paleoclimate studies suggest a strong interhemispheric temperature gradient as the trigger for changes in the Pacific Ocean. For example, there is evidence that during the Little Ice Age a southward migration of the ITCZ coincided with an intensified Walker circulation, westward shifted precipitation (Yan et al. 2015) and also reduced El Niño frequency (Sachs et al. 2009). Moreover, cooler mean central equatorial Pacific conditions have been found in proxies during the Last Glacial Maximum (Monteagudo et al. 2021), which is also a period with an enhanced interhemispheric gradient forcing, although during that climate epoch it is difficult to separate out the effects of mean global cooling from internal Pacific changes.

When analyzing ENSO diversity in the AMOC-off simulations, we found a notable reduction in the frequency of EP ENSO events relative to the frequency of CP ENSO events. This appears consistent with the greater reduction in the thermocline feedback compared to the zonal advective feedback, which are respectively the more important feedbacks for EP and CP ENSO (Kug et al. 2009; Yu et al. 2010; Xie and Jin 2018). The reduction in these positive feedbacks is offset by the weakened thermodynamical damping, which tends to have a greater impact on CP events due to the higher sensitivity of heat fluxes to a small SST anomaly in the central/west Pacific (Kang and Kug 2002). This could explain the slight increase in CP frequency, consistent with the findings by (Svendsen et al. 2013), who show a tendency for ENSO to shift to the CP type in a weakened AMOC simulation.

Furthermore, in the altered mean tropical Pacific state under AMOC-off, the reduced SST variability causes the temperature not to exceed the convective threshold as often as it does in the AMOC-on case (despite the convective threshold itself reducing by ~1°C). This is reflected in a decline in the frequency of strong El Niño events in AMOC-off. All these ENSO dynamical changes ultimately lead to a reduction in the nonlinearity and asymmetry of ENSO when the AMOC is collapsed.

Since the AMOC has shut down in the past (e.g., Clement and Peterson 2008) and it is projected to slow down under increasing greenhouse gases (Collins et al. 2013), a collapsed AMOC is not a discarded possibility in a future warming world (Bakker et al. 2016; Liu et al. 2017). Moreover, current generation climate models still do not represent the effect of land ice melt (Eyring et al. 2016), which would contribute to a further AMOC decline via salinity changes in the North Atlantic (Golledge et al. 2019). Thus, our study is relevant for both ENSO paleoclimate studies as well as future climate projections. In paleo studies, there are still open questions about the AMOC's role in ENSO changes (Lu et al. 2018). In future projection studies, a diverse response in ENSO has been documented; for example, an increased frequency of CP El Niño events (Yeh et al. 2009) and extreme El Niño/La Niña events (Cai et al. 2014, 2020) and an overall increase in variability of EP and CP ENSO in CMIP6 models (Cai et al. 2021). An important aspect to consider that could have implications for these studies is that the representation of interbasin interactions tends to be underestimated in climate models, and the interbasin coupling varies across models (Kajtar et al. 2017; Cai et al. 2019). While the model used in this present study is skillful in this regard (Orihuela-Pinto et al. 2022), this complex issue warrants further investigation. Understanding all the factors that contribute to these differing responses across models, and model deficiencies, is important to better comprehend the past and future behavior of ENSO. This study sheds light on these issues by demonstrating how an AMOC collapse can lead to a reduction in the frequency of extreme El Niño events and increased occurrences of CP events.

Acknowledgments. This study was supported by the Australian Research Council (ARC Grants CE110001028 and FT160100495). M.H.E., A.S., and A.S.T. are supported by the Earth Science and Climate Change Hub of the Australian Government's National Environmental Science Program (NESP). M.H.E. and A.S. are also supported by the Centre for Southern Hemisphere Oceans Research (CSHOR), a joint research center between QNLM, CSIRO, UNSW, and UTAS. We thank the computational resources provided by the Australian National Computational Infrastructure (NCI) National Facility.

Unauthenticated | Downloaded 01/24/24 02:17 AM UTC

REFERENCES

Bakker, P., and Coauthors, 2016: Fate of the Atlantic meridional overturning circulation: Strong decline under continued warming and Greenland melting. *Geophys. Res. Lett.*, **43**, 12 252–12 260, https://doi.org/10.1002/2016GL070457.

Bryden, H. L., H. R. Longworth, and S. A. Cunningham, 2005: Slowing of the Atlantic meridional overturning circulation at 25°N. *Nature*, **438**, 655–657, https://doi.org/10.1038/nature04385.

Caesar, L., S. Rahmstorf, A. Robinson, G. Feulner, and V. Saba, 2018: Observed fingerprint of a weakening Atlantic Ocean overturning circulation. *Nature*, **556**, 191–196, https://doi.org/10.1038/s41586-018-0006-5.

——, G. D. McCarthy, D. J. R. Thornalley, N. Cahill, and S. Rahmstorf, 2021: Current Atlantic meridional overturning circulation weakest in last millennium. *Nat. Geosci.*, **14**, 118–120, https://doi.org/10.1038/s41561-021-00699-z.

Cai, W., and Coauthors, 2014: Increasing frequency of extreme El Niño events due to greenhouse warming. *Nat. Climate Change*, **4**, 111–116, https://doi.org/10.1038/nclimate2100.

——, G. Wang, A. Santoso, X. Lin, and L. Wu, 2017: Definition of extreme El Niño and its impact on projected increase in extreme El Niño frequency. *Geophys. Res. Lett.*, **44**, 11 184–11 190, https://doi.org/10.1002/2017GL075635.

——, and Coauthors, 2018: Increased variability of eastern Pacific El Niño under greenhouse warming. *Nature*, **564**, 201–206, https://doi.org/10.1038/s41586-018-0776-9.

——, and Coauthors, 2019: Pantropical climate interactions. *Science*, **363**, eaav4236, https://doi.org/10.1126/science.aav4236.

——, A. Santoso, G. Wang, L. Wu, M. Collins, M. Lengaigne, S. Power, and A. Timmermann, 2020: ENSO response to greenhouse forcing. *El Niño Southern Oscillation in a Changing Climate, Geophys. Monogr.*, Vol. 253, Amer. Geophys. Union, 289–307.

——, and Coauthors, 2021: Changing El Niño–Southern Oscillation in a warming climate. *Nat. Rev. Earth Environ.*, **2**, 628–644, https://doi.org/10.1038/s43017-021-00199-z.

Capotondi, A., 2013: ENSO diversity in the NCAR CCSM4 climate model. *J. Geophys. Res. Oceans*, **118**, 4755–4770, https://doi.org/10.1002/jgrc.20335.

——, and Coauthors, 2015: Understanding ENSO diversity. *Bull. Amer. Meteor. Soc.*, **96**, 921–938, https://doi.org/10.1175/BAMS-D-13-00117.1.

Cessi, P., K. Bryan, and R. Zhang, 2004: Global seiching of thermocline waters between the Atlantic and the Indian-Pacific Ocean basins. *Geophys. Res. Lett.*, **31**, L04302, https://doi.org/10.1029/2003GL019091.

Chang, P., B. Wang, T. Li, and L. Ji, 1994: Interactions between the seasonal cycle and the Southern Oscillation—Frequency entrainment and chaos in a coupled ocean-atmosphere model. *Geophys. Res. Lett.*, **21**, 2817–2820, https://doi.org/10.1029/94GL02759.

——, L. Zhang, R. Saravanan, D. J. Vimont, J. C. H. Chiang, L. Ji, H. Seidel, and M. K. Tippett, 2007: Pacific meridional mode and El Niño–Southern Oscillation. *Geophys. Res. Lett.*, **34**, L16608, https://doi.org/10.1029/2007GL030302.

Cheng, W., C. M. Bitz, and J. C. H. Chiang, 2007: Adjustment of the global climate to an abrupt slowdown of the Atlantic meridional overturning circulation. *Ocean Circulation: Mechanisms and Impacts—Past and Future Changes of Meridional Overturning*, Wiley, 295–313.

Clark, P. U., N. G. Pisias, T. F. Stocker, and A. J. Weaver, 2002: The role of the thermohaline circulation in abrupt climate change. *Nature*, **415**, 863–869, https://doi.org/10.1038/415863a.

Clement, A. C., and L. C. Peterson, 2008: Mechanisms of abrupt climate change of the last glacial period. *Rev. Geophys.*, **46**, RG4002, https://doi.org/10.1029/2006RG000204.

Collins, M., and Coauthors, 2013: Long-term climate change: Projections, commitments and irreversibility. *Climate Change 2013: The Physical Science Basis*, T. F. Stocker et al., Eds., Cambridge University Press, 1029–1136.

Danabasoglu, G., S. G. Yeager, Y. O. Kwon, J. J. Tribbia, A. S. Phillips, and J. W. Hurrell, 2012: Variability of the Atlantic meridional overturning circulation in CCSM4. *J. Climate*, **25**, 5153–5172, https://doi.org/10.1175/JCLI-D-11-00463.1.

Deser, C., M. A. Alexander, S.-P. Xie, and A. S. Phillips, 2010: Sea surface temperature variability: Patterns and mechanisms. *Annu. Rev. Mar. Sci.*, **2**, 115–143, https://doi.org/10.1146/annurev-marine-120408-151453.

——, and Coauthors, 2012: ENSO and Pacific decadal variability in the Community Climate System Model version 4. *J. Climate*, **25**, 2622–2651, https://doi.org/10.1175/JCLI-D-11-00301.1.

Dong, B., and R. T. Sutton, 2007: Enhancement of ENSO variability by a weakened Atlantic thermohaline circulation in a coupled GCM. *J. Climate*, **20**, 4920–4939, https://doi.org/10.1175/JCLI4284.1.

Emile-Geay, J., and Coauthors, 2016: Links between tropical Pacific seasonal, interannual and orbital variability during the Holocene. *Nat. Geosci.*, **9**, 168–173, https://doi.org/10.1038/ngeo2608.

Enfield, D. B., A. M. Mestas-Nuñez, and P. J. Trimble, 2001: The Atlantic multidecadal oscillation and its relation to rainfall and river flows in the continental U.S. *Geophys. Res. Lett.*, **28**, 2077–2080, https://doi.org/10.1029/2000GL012745.

Eyring, V., S. Bony, G. A. Meehl, C. A. Senior, B. Stevens, R. J. Stouffer, and K. E. Taylor, 2016: Overview of the Coupled Model Intercomparison Project Phase 6 (CMIP6) experimental design and organization. *Geosci. Model Dev.*, **9**, 1937–1958, https://doi.org/10.5194/gmd-9-1937-2016.

Freund, M. B., B. J. Henley, D. J. Karoly, H. V. McGregor, N. J. Abram, and D. Dommenget, 2019: Higher frequency of central Pacific El Niño events in recent decades relative to past centuries. *Nat. Geosci.*, **12**, 450–455, https://doi.org/10.1038/s41561-019-0353-3.

Frierson, D. M. W., and Coauthors, 2013: Contribution of ocean overturning circulation to tropical rainfall peak in the Northern Hemisphere. *Nat. Geosci.*, **6**, 940–944, https://doi.org/10.1038/ngeo1987.

Geng, T., W. Cai, and L. Wu, 2020: Two types of ENSO varying in tandem facilitated by nonlinear atmospheric convection. *Geophys. Res. Lett.*, **47**, e2020GL088784, https://doi.org/10.1029/2020GL088784.

Gent, P. R., and Coauthors, 2011: The Community Climate System Model Version 4. *J. Climate*, **24**, 4973–4991, https://doi.org/10.1175/2011JCLI4083.1.

Golledge, N. R., E. D. Keller, N. Gomez, K. A. Naughten, J. Bernales, L. D. Trusel, and T. L. Edwards, 2019: Global environmental consequences of twenty-first-century ice-sheet melt. *Nature*, **566**, 65–72, https://doi.org/10.1038/s41586-019-0889-9.

Hoerling, M. P., A. Kumar, and M. Zhong, 1997: El Niño, La Niña, and the nonlinearity of their teleconnections. *J. Climate*, **10**, 1769–1786, https://doi.org/10.1175/1520-0442(1997)010<1769:ENOLNA>2.0.CO;2.

Unauthenticated | Downloaded 01/24/24 02:17 AM UTC

Huang, B., and Coauthors, 2017: Extended Reconstructed Sea Surface Temperature, version 5 (ERSSTv5): Upgrades, validations, and intercomparisons. *J. Climate*, **30**, 8179–8205, https://doi.org/10.1175/JCLI-D-16-0836.1.

Jin, F. F., 1997: An equatorial ocean recharge paradigm for ENSO. Part I: Conceptual model. *J. Atmos. Sci.*, **54**, 811–829, https://doi.org/10.1175/1520-0469(1997)054<0811:AEORPF>2.0.CO;2.

——, S. T. Kim, and L. Bejarano, 2006: A coupled-stability index for ENSO. *Geophys. Res. Lett.*, **33**, L23708, https://doi.org/10.1029/2006GL027221.

Johnson, N. C., and S.-P. Xie, 2010: Changes in the sea surface temperature threshold for tropical convection. *Nat. Geosci.*, **3**, 842–845, https://doi.org/10.1038/ngeo1008.

Kajtar, J. B., A. Santoso, M. H. England, and W. Cai, 2017: Tropical climate variability: Interactions across the Pacific, Indian, and Atlantic Oceans. *Climate Dyn.*, **48**, 2173–2190, https://doi.org/10.1007/s00382-016-3199-z.

Kang, I. S., and J. S. Kug, 2002: EI Niño and la Niña sea surface temperature anomalies: Asymmetry characteristics associated with their wind stress anomalies. *J. Geophys. Res.*, **107**, 4372, https://doi.org/10.1029/2001JD000393.

Karamperidou, C., F.-F. Jin, and J. L. Conroy, 2017: The importance of ENSO nonlinearities in tropical pacific response to external forcing. *Climate Dyn.*, **49**, 2695–2704, https://doi.org/10.1007/s00382-016-3475-y.

——, and Coauthors, 2020: ENSO in a changing climate: Challenges, Paleo-perspectives, and outlook. *El Niño Southern Oscillation in a Changing Climate, Geophys. Monogr.*, Vol. 253, Amer. Geophys. Union, 471–484.

Kim, S. T., and F. F. Jin, 2011: An ENSO stability analysis. Part I: Results from a hybrid coupled model. *Climate Dyn.*, **36**, 1593–1607, https://doi.org/10.1007/s00382-010-0796-0.

——, W. Cai, F. F. Jin, and J. Y. Yu, 2014: ENSO stability in coupled climate models and its association with mean state. *Climate Dyn.*, **42**, 3313–3321, https://doi.org/10.1007/s00382-013-1833-6.

Kug, J.-S., F.-F. Jin, and S.-I. An, 2009: Two types of El Niño events: Cold tongue El Niño and warm Pool El Niño. *J. Climate*, **22**, 1499–1515, https://doi.org/10.1175/2008JCLI2624.1.

Liao, H., C. Wang, and Z. Song, 2021: ENSO phase-locking biases from the CMIP5 to CMIP6 models and a possible explanation. *Deep-Sea Res. II*, **189–190**, 104943, https://doi.org/10.1016/j.dsr2.2021.104943.

Liguori, G., and E. Di Lorenzo, 2018: Meridional modes and increasing Pacific decadal variability under anthropogenic forcing. *Geophys. Res. Lett.*, **45**, 983–991, https://doi.org/10.1002/2017GL076548.

Liu, W., S.-P. Xie, Z. Liu, and J. Zhu, 2017: Overlooked possibility of a collapsed Atlantic meridional overturning circulation in warming climate. *Sci. Adv.*, **3**, e1601666, https://doi.org/10.1126/sciadv.1601666.

Liu, Z., 2002: A simple model study of ENSO suppression by external periodic forcing. *J. Climate*, **15**, 1088–1098, https://doi.org/10.1175/1520-0442(2002)015<1088:ASMSOE>2.0.CO;2.

——, Z. Lu, X. Wen, B. L. Otto-Bliesner, A. Timmermann, and K. M. Cobb, 2014: Evolution and forcing mechanisms of El Niño over the past 21 000 years. *Nature*, **515**, 550–553, https://doi.org/10.1038/nature13963.

Lu, Z., Z. Liu, J. Zhu, and K. M. Cobb, 2018: A review of paleo El Niño–Southern Oscillation. *Atmosphere*, **9**, 130, https://doi.org/10.3390/atmos9040130.

Lübbecke, J. F., and M. J. McPhaden, 2013: A comparative stability analysis of Atlantic and Pacific Niño modes. *J. Climate*, **26**, 5965–5980, https://doi.org/10.1175/JCLI-D-12-00758.1.

Mahajan, S., R. Zhang, and T. L. Delworth, 2011: Impact of the Atlantic meridional overturning circulation (AMOC) on Arctic surface air temperature and sea ice variability. *J. Climate*, **24**, 6573–6581, https://doi.org/10.1175/2011JCLI4002.1.

Marshall, J., A. Donohoe, D. Ferreira, and D. McGee, 2014: The ocean's role in setting the mean position of the inter-tropical convergence zone. *Climate Dyn.*, **42**, 1967–1979, https://doi.org/10.1007/s00382-013-1767-z.

Martin, E. R., C. Thorncroft, and B. B. Booth, 2014: The multidecadal Atlantic SST–Sahel rainfall teleconnection in CMIP5 simulations. *J. Climate*, **27**, 784–806, https://doi.org/10.1175/JCLI-D-13-00242.1.

McKenna, S., A. Santoso, A. Sen Gupta, A. S. Taschetto, and W. Cai, 2020: Indian Ocean dipole in CMIP5 and CMIP6: Characteristics, biases, and links to ENSO. *Sci. Rep.*, **10**, 11 500, https://doi.org/10.1038/s41598-020-68268-9.

McPhaden, M. J., S. E. Zebiak, and M. H. Glantz, 2006: ENSO as an integrating concept in Earth science. *Science*, **314**, 1740–1745, https://doi.org/10.1126/science.1132588.

Monteagudo, M. M., J. Lynch-Stieglitz, T. M. Marchitto, and M. W. Schmidt, 2021: Central equatorial Pacific cooling during the last glacial maximum. *Geophys. Res. Lett.*, **48**, e2020GL088592, https://doi.org/10.1029/2020gl088592.

Orihuela-Pinto, B., M. H. England, and A. S. Taschetto, 2022: Interbasin and interhemispheric impacts of a collapsed Atlantic overturning circulation. *Nat. Climate Change*, **12**, 558–565, https://doi.org/10.1038/s41558-022-01380-y.

Rahmstorf, S., 2002: Ocean circulation and climate during the past 120 000 years. *Nature*, **419**, 207–214, https://doi.org/10.1038/nature01090.

——, J. E. Box, G. Feulner, M. E. Mann, A. Robinson, S. Rutherford, and E. J. Schaffernicht, 2015: Exceptional twentieth-century slowdown in Atlantic Ocean overturning circulation. *Nat. Climate Change*, **5**, 475–480, https://doi.org/10.1038/nclimate2554.

Rainsley, E., L. Menviel, C. J. Fogwill, C. S. M. Turney, A. L. C. Hughes, and D. H. Rood, 2018: Greenland ice mass loss during the Younger Dryas driven by Atlantic meridional overturning circulation feedbacks. *Sci. Rep.*, **8**, 11 307, https://doi.org/10.1038/s41598-018-29226-8.

Rayner, N. A., D. E. Parker, E. B. Horton, C. K. Folland, L. V. Alexander, D. P. Rowell, E. C. Kent, and A. Kaplan, 2003: Global analyses of sea surface temperature, sea ice, and night marine air temperature since the late nineteenth century. *J. Geophys. Res.*, **108**, 4407, https://doi.org/10.1029/2002JD002670.

Sachs, J. P., D. Sachse, R. H. Smittenberg, Z. Zhang, D. S. Battisti, and S. Golubic, 2009: Southward movement of the Pacific intertropical convergence zone AD 1400–1850. *Nat. Geosci.*, **2**, 519–525, https://doi.org/10.1038/ngeo554.

Santoso, A., M. H. England, and W. Cai, 2012: Impact of Indo-Pacific feedback interactions on ENSO dynamics diagnosed using ensemble climate simulations. *J. Climate*, **25**, 7743–7763, https://doi.org/10.1175/JCLI-D-11-00287.1.

——, and Coauthors, 2019: Dynamics and predictability of El Niño–Southern Oscillation: An Australian perspective on progress and challenges. *Bull. Amer. Meteor. Soc.*, **100**, 403–420, https://doi.org/10.1175/BAMS-D-18-0057.1.

Song, Z., H. Liu, and X. Chen, 2020: Eastern equatorial Pacific SST seasonal cycle in global climate models: From CMIP5 to

Unauthenticated | Downloaded 01/24/24 02:17 AM UTC

CMIP6. *Acta Oceanol. Sin.*, **39**, 50–60, https://doi.org/10.1007/s13131-020-1623-z.

Stein, K., N. Schneider, A. Timmermann, and F. F. Jin, 2010: Seasonal synchronization of ENSO events in a linear stochastic model. *J. Climate*, **23**, 5629–5643, https://doi.org/10.1175/2010JCLI3292.1.

Stouffer, R. J., and Coauthors, 2006: Investigating the causes of the response of the thermohaline circulation to past and future climate changes. *J. Climate*, **19**, 1365–1387, https://doi.org/10.1175/JCLI3689.1.

Sutton, R. T., and D. L. R. Hodson, 2005: Atlantic Ocean forcing of North American and European summer climate. *Science*, **309**, 115–118, https://doi.org/10.1126/science.1109496.

Svendsen, L., N. G. Kvamstø, and N. Keenlyside, 2013: Weakening AMOC connects equatorial Atlantic and Pacific interannual variability. *Climate Dyn.*, **43**, 2931–2941, https://doi.org/10.1007/s00382-013-1904-8.

Takahashi, K., and B. Dewitte, 2016: Strong and moderate nonlinear El Niño regimes. *Climate Dyn.*, **46**, 1627–1645, https://doi.org/10.1007/s00382-015-2665-3.

——, A. Montecinos, K. Goubanova, and B. Dewitte, 2011: ENSO regimes: Reinterpreting the canonical and Modoki El Niño. *Geophys. Res. Lett.*, **38**, L10704, https://doi.org/10.1029/2011GL047364.

Taschetto, A. S., A. Sen Gupta, N. C. Jourdain, A. Santoso, C. C. Ummenhofer, and M. H. England, 2014: Cold tongue and warm pool ENSO events in CMIP5: Mean state and future projections. *J. Climate*, **27**, 2861–2885, https://doi.org/10.1175/JCLI-D-13-00437.1.

Timmermann, A., S.-I. An, U. Krebs, and H. Goosse, 2005: ENSO suppression due to weakening of the North Atlantic thermohaline circulation. *J. Climate*, **18**, 3122–3139, https://doi.org/10.1175/JCLI3495.1.

——, and Coauthors, 2007a: The influence of a weakening of the Atlantic meridional overturning circulation on ENSO. *J. Climate*, **20**, 4899–4919, https://doi.org/10.1175/JCLI4283.1.

——, S. J. Lorenz, S.-I. An, A. Clement, and S.-P. Xie, 2007b: The effect of orbital forcing on the mean climate and variability of the tropical Pacific. *J. Climate*, **20**, 4147–4159, https://doi.org/10.1175/JCLI4240.1.

——, and Coauthors, 2018: El Niño–Southern Oscillation complexity. *Nature*, **559**, 535–545, https://doi.org/10.1038/s41586-018-0252-6.

Trenberth, K. E., 2020: ENSO in the global climate system. *El Niño Southern Oscillation in a Changing Climate, Geophys. Monogr.*, Vol. 253, Amer. Geophys. Union, 21–37.

Vellinga, M., and R. A. Wood, 2002: Global climatic impacts of a collapse of the Atlantic thermohaline circulation. *Climatic Change*, **54**, 251–267, https://doi.org/10.1023/A:1016168827653.

Wang, B., X. Luo, Y. M. Yang, W. Sun, M. A. Cane, W. Cai, S. W. Yeh, and J. Liu, 2019: Historical change of El Niño properties sheds light on future changes of extreme El Niño. *Proc. Natl. Acad. Sci. USA*, **116**, 22 512–22 517, https://doi.org/10.1073/pnas.1911130116.

Williamson, M. S., M. Collins, S. S. Drijfhout, R. Kahana, J. V. Mecking, and T. M. Lenton, 2018: Effect of AMOC collapse on ENSO in a high resolution general circulation model. *Climate Dyn.*, **50**, 2537–2552, https://doi.org/10.1007/s00382-017-3756-0.

Wu, L., C. Li, C. Yang, and S.-P. Xie, 2008: Global teleconnections in response to a shutdown of the Atlantic meridional overturning circulation. *J. Climate*, **21**, 3002–3019, https://doi.org/10.1175/2007JCLI1858.1.

Xie, R., and F. F. Jin, 2018: Two leading ENSO modes and El Niño types in the Zebiak–Cane model. *J. Climate*, **31**, 1943–1962, https://doi.org/10.1175/JCLI-D-17-0469.1.

Xie, S.-P., 1994: On the genesis of the equatorial annual cycle. *J. Climate*, **7**, 2008–2013, https://doi.org/10.1175/1520-0442(1994)007<2008:OTGOTE>2.0.CO;2.

Yan, H., W. Wei, W. Soon, Z. An, W. Zhou, Z. Liu, Y. Wang, and R. M. Carter, 2015: Dynamics of the intertropical convergence zone over the western Pacific during the Little Ice Age. *Nat. Geosci.*, **8**, 315–320, https://doi.org/10.1038/ngeo2375.

Yeh, S.-W., J.-S. Kug, B. Dewitte, M.-H. Kwon, B. P. Kirtman, and F.-F. Jin, 2009: El Niño in a changing climate. *Nature*, **461**, 511–514, https://doi.org/10.1038/nature08316.

——, and Coauthors, 2018: ENSO atmospheric teleconnections and their response to greenhouse gas forcing. *Rev. Geophys.*, **56**, 185–206, https://doi.org/10.1002/2017RG000568.

Yu, J. Y., H. Y. Kao, and T. Lee, 2010: Subtropics-related interannual sea surface temperature variability in the central equatorial Pacific. *J. Climate*, **23**, 2869–2884, https://doi.org/10.1175/2010JCLI3171.1.

Yun, K.-S., J.-Y. Lee, A. Timmermann, K. Stein, M. F. Stuecker, J. C. Fyfe, and E.-S. Chung, 2021: Increasing ENSO–rainfall variability due to changes in future tropical temperature–rainfall relationship. *Commun. Earth Environ.*, **2**, 43, https://doi.org/10.1038/s43247-021-00108-8.

Zhang, H., A. Clement, and P. Di Nezio, 2014: The South Pacific meridional mode: A mechanism for ENSO-like variability. *J. Climate*, **27**, 769–783, https://doi.org/10.1175/JCLI-D-13-00082.1.

Zhang, R., and T. L. Delworth, 2005: Simulated tropical response to a substantial weakening of the Atlantic thermohaline circulation. *J. Climate*, **18**, 1853–1860, https://doi.org/10.1175/JCLI3460.1.

Unauthenticated | Downloaded 01/24/24 02:17 AM UTC